Noncritical quadrature squeezing in two-transverse-mode optical parametric oscillators

Carlos Navarrete-Benlloch,[1] Alejandro Romanelli,[2] Eugenio Roldán,[1] and Germán J. de Valcárcel[1]
[1]*Departament d'Òptica, Universitat de València, Dr. Moliner 50, 46100 Burjassot, Spain*
[2]*Instituto de Física, Facultad de Ingeniería Universidad de la República, C.C. 30, C.P. 11000 Montevideo, Uruguay*
(Received 8 October 2009; published 22 April 2010)

In this article we explore the quantum properties of a degenerate optical parametric oscillator when it is tuned to the first family of transverse modes at the down-converted frequency. Recently we found [C. Navarrete-Benlloch *et al.*, Phys. Rev. Lett. **100**, 203601 (2008)] that above threshold a TEM_{10} mode following a random rotation in the transverse plane emerges in this system (we denote it as the *bright* mode), breaking thus its rotational invariance. Then, owing to the mode orientation being undetermined, we showed that the phase quadrature of the transverse mode orthogonal to this one (denoted as the *dark* mode) is perfectly squeezed at any pump level and without an increase in the fluctuations on its amplitude quadrature (which seems to contradict the uncertainty principle). In this article we go further in the study of this system and analyze some important features not considered previously. First we show that the apparent violation of the uncertainty principle is just that—"apparent"—as the conjugate pair of the squeezed quadrature is not another quadrature but the orientation of the bright mode (which is completely undetermined in the long term). We also study a homodyne scheme in which the local oscillator is not perfectly matched to the dark mode, as this could be impossible in real experiments due to the random rotation of the mode, showing that even in this case large levels of noise reduction can be obtained (also including the experimentally unavoidable phase fluctuations). Finally, we show that neither the adiabatic elimination of the pump variables nor the linearization of the quantum equations are responsible for the remarkable properties of the dark mode (which we prove analytically and through numerical simulations, respectively), which were simplifying assumptions used in Navarrete-Benlloch *et al.* [Phys. Rev. Lett. **100**, 203601 (2008)]. These studies show that the production of noncritically squeezed light through spontaneous rotational symmetry breaking is a robust phenomenon.

DOI: 10.1103/PhysRevA.81.043829 PACS number(s): 42.50.Dv, 42.50.Lc, 42.50.Tx, 42.65.Yj

I. INTRODUCTION

One of the most amazing predictions offered by the quantum theory of light is what has been called *vacuum fluctuations*: Even in absence of photons (vacuum), the value of the fluctuations of some observables are different from zero. These fluctuations cannot be removed by improving the experimental instrumental, and hence, they are a source of nontechnical noise (*quantum noise*), which seems to establish a limit for the precision of experiments involving light.

During the late 1970s and mid-1980s, ways for overcoming this fundamental limit were predicted and experimentally demonstrated [1]. In the case of the quadratures of light (equivalent to the position and momentum of a harmonic oscillator), the trick was to eliminate (*squeeze*) quantum noise from one quadrature at the expense of increasing the noise of its canonically conjugated one in order to preserve their Heisenberg uncertainty relation. States with this property are called *squeezed states*, and they can be generated by means of nonlinear optical processes. In particular, the largest levels of squeezing are obtained by using nonlinear resonators operating near threshold, this level being degraded quickly as one moves away from that critical point.

To date, the best squeezing ever achieved is a 90% of noise reduction with respect to vacuum (the so-called *standard quantum limit*) [2,3], and *degenerate optical parametric oscillators* (DOPOs) have been used to this end. A DOPO consists on a nonlinear $\chi^{(2)}$ crystal placed inside an optical cavity; when pumped above some threshold level with a laser beam at frequency $2\omega_0$, a field oscillating at half that frequency (*signal* frequency) is generated. A linearized analysis of the DOPO's quantum fluctuations reveals that the phase quadrature of the signal field can be perfectly squeezed when the pump's power is tuned to the DOPO's threshold value [4]. Of course, ideal perfect squeezing cannot be real in this case, as it would entail an infinite number of photons in the generated mode, and it can be shown that nonlinear corrections make this squeezing level become finite [5].

Apart from fundamental reasons, improving the quality of squeezed light is an important task because of its applications. For example, in the fields of *quantum information with continuous variables* [6] (as mixing squeezed beams with beam splitters offers the possibility to generate multipartite entangled beams [7]) and *high-precision measurements* (such as beam displacement and pointing measurements [8] and gravitational wave detection [9]), applications of squeezed light have been theoretically and experimentally demonstrated.

Recently, our group has developed a strategy that would lead to the generation of light with a high level of squeezing at any pump level above threshold in DOPOs (*noncritically squeezed light*). The idea is to allow for the existence of several transverse modes at the signal frequency in a DOPO possessing some spatial symmetry in the transverse plane (e.g., rotational or translational); under some circumstances, a pattern breaking the corresponding spatial symmetry can be generated, and quantum noise can randomly move it along the invariant direction (i.e., rotate or translate it in the transverse plane). This can be seen as an indefiniteness in the transverse position of the generated pattern, which, invoking now the uncertainty principle, could be accompanied by the perfect determination of its associated momentum (angular or linear). Hence, we

 ©2010 The American Physical Society

could expect noise reduction in the empty pattern coinciding with the momentum of the generated pattern. Moreover, as this is related to the spontaneous symmetry breaking, the perfect squeezing should occur at any pump level above threshold.

In Ref. [10], the translational symmetry breaking was considered in broad-area, planar DOPOs, where cavity solitons (CSs), as well as extended patterns, have been predicted to exist [11]. It was shown that all the preceding reasoning is true: The position of the CS diffuses in the transverse plane, and the phase quadrature of the pattern coinciding with its linear momentum (namely, its $\pi/2$ phase-shifted transverse gradient) is perfectly squeezed (within the linearized theory) at any pump level above threshold. The problem of this model is that it is not too close to current experimental setups and even CSs have not yet been observed in DOPOs.

This was one of the reasons why the theory of a simpler system was developed in Ref. [12]: a rotationally symmetric DOPO tuned to the first family of transverse modes at the signal frequency [13,14]. The first transverse-mode family supports Laguerre-Gauss (LG) modes $L_{\pm1}(\mathbf{r})$ with ±1 orbital angular momentum (OAM), where $\mathbf{r}=(x,y)$ are the transverse coordinates. When pumped with a Gaussian mode with zero OAM, two signal photons with opposite OAM are generated in the $\chi^{(2)}$ crystal. Alternatively, the simultaneous generation of one $L_{+1}(\mathbf{r})$ photon and another $L_{-1}(\mathbf{r})$ one corresponds to the generation of two Hermite-Gauss (HG) TEM_{10} photons, the orientation of this TEM_{10} mode (θ in Fig. 1) given by half the phase difference between the subjacent $L_{\pm1}(\mathbf{r})$ modes. Again in this case, we proved our reasoning given previously: Quantum noise is able to rotate randomly this bright mode, and the phase quadrature of its angular momentum (its $-\pi/2$ phase shifted angular derivative), which corresponds in this case to another HG mode orthogonal to the generated one (we will refer to it as the dark mode), is perfectly squeezed within the linearized theory and at any pump level above threshold. In addition, we showed that this result is quite robust against deviations from the perfect rotational invariance of the DOPO.

Moreover, a surprising result was found: Although the phase quadrature of the dark mode is perfectly squeezed, its corresponding amplitude quadrature has not increased uncertainty; that is, the quadratures of this rotating mode do not form a canonical pair. We intuitively explained this by noting that the excess of noise is transferred not to another quadrature, but to the orientation θ of the pattern, which actually is the canonical pair of the squeezed quadrature; in the present article we prove this statement by using the arguments developed in Ref. [15].

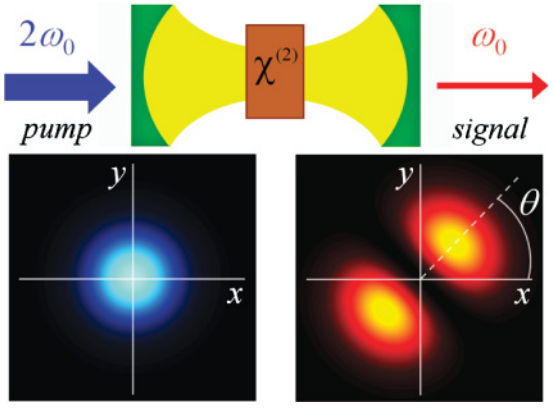

FIG. 1. (Color online) Scheme of the two-transverse-mode DOPO.

Indeed, the study of this rotationally symmetric DOPO was carried out under some assumptions whose repercussions will be analyzed in the current article. First, we supposed that cavity losses at the signal frequency were small compared with that at the pump frequency, which allowed us to adiabatically eliminate the pump variables. Next, the usual linearization of the nonlinear Langevin equations around their classical stationary solution was done. Finally, in order to prove the noncritical squeezing we proposed a homodyne detection scheme in which the local oscillator was a TEM_{10} mode matched to the dark mode at any time; that is, it was following the random rotation of this mode, an ideal situation that is not possible in real experiments.

Now let us summarize what we are going to show in this article, which is divided into four main parts. In the first one (Sec. II), we describe the DOPO tuned to the first transverse family (the *two-transverse-mode DOPO*) and find its associated quantum Langevin equations. In Sec. III, we study the classical emission of the system and show how the rotational symmetry is broken by the generated transverse pattern. Section IV is the main section of the article: The quantum properties of the DOPO are analyzed by linearizing the Langevin equations. Here we will prove the random rotation of the classical pattern and find the squeezing properties of the bright and dark modes. In addition, we will show that the quadratures of the dark mode do not form a canonical set, but they are canonically related to the pattern orientation (where the excess of noise goes). We close this section by analyzing the repercussion of keeping fixed the orientation of the local oscillator, showing that even in this case large levels of squeezing can be obtained. In the last part (Sec. V) we show that the approximations considered in the previous sections (the adiabatic elimination of the pump and the linearization procedure) are not responsible for the remarkable squeezing properties of the dark mode, as they follow directly from the spontaneous rotational symmetry breaking. At the end (Sec. VI) we give some conclusions. In order to make clearer the physics behind the phenomenon, we have left most of the technical details to appendices.

II. DESCRIPTION OF THE TWO-TRANSVERSE-MODE DOPO

A. The field inside the cavity

One of the simplest configurations of the DOPO's cavity allowing for the generation of a rotationally asymmetric pattern is the following [12]: At some phase-matched frequency $2\omega_0$ it is tuned to a fundamental Gaussian transverse mode $G(\mathbf{r})$, while at half that frequency, ω_0, the first transverse family is resonant. In the first transverse family two Laguerre-Gauss modes exist, $L_{\pm1}(\mathbf{r})$. The exact expression of the modes in the waist plane of the resonator (where the $\chi^{(2)}$ crystal is placed)

is given by [16]

$$G(\mathbf{r}) = \sqrt{\frac{2}{\pi}}\frac{1}{w_\mathrm{p}} e^{-\frac{r^2}{w_\mathrm{p}^2}},$$
$$L_{\pm 1}(\mathbf{r}) = \frac{2}{\sqrt{\pi}}\frac{r}{w_\mathrm{s}^2} e^{-\frac{r^2}{w_\mathrm{s}^2}} e^{\pm i\phi}, \tag{1}$$

where $\mathbf{r} = r(\cos\phi, \sin\phi)$ is the coordinate vector in the transverse plane, and w_i is the beam radius at the waist plane, which depends on the cavity geometry and the resonance frequency of the mode (see Appendix A).

These transverse modes have 0 and ± 1 OAM, respectively, as they are eigenmodes of the OAM operator $-i\partial_\phi$ with those eigenvalues.

The field inside the cavity can be written then as

$$\hat{E} = i\mathcal{F}_\mathrm{p}\hat{A}_\mathrm{p}(\mathbf{r},t)e^{-2i\omega_0 t} + i\mathcal{F}_\mathrm{s}\hat{A}_\mathrm{s}(\mathbf{r},t)e^{-i\omega_0 t} + \mathrm{H.c.}, \tag{2}$$

with

$$\mathcal{F}_\mathrm{p} = \sqrt{2}\mathcal{F}_\mathrm{s} = \sqrt{\frac{2\hbar\omega_0}{n\varepsilon_0 L}}, \tag{3}$$

n being the refractive index of the crystal, and L the effective cavity length (H.c. stands for "Hermitian conjugate"). The slowly varying envelopes are given by

$$\hat{A}_\mathrm{p}(\mathbf{r},t) = \hat{a}_0(t)G(\mathbf{r}), \tag{4a}$$
$$\hat{A}_\mathrm{s}(\mathbf{r},t) = \hat{a}_{+1}(t)L_{+1}(\mathbf{r}) + \hat{a}_{-1}(t)L_{-1}(\mathbf{r}), \tag{4b}$$

where the boson operators satisfy the usual equal-time commutation relations:

$$[\hat{a}_m(t), \hat{a}_n^\dagger(t)] = \delta_{mn};\ m,n = 0,\pm 1. \tag{5}$$

Instead of using the LG basis, one can work in the most usual TEM$_{mn}$ (HG) basis. Denoting by $H_{10}^\psi(\mathbf{r})$ and $H_{01}^\psi(\mathbf{r})$ a TEM$_{10}$ mode rotated an angle ψ with respect to the x axis and its orthogonal, these are given by

$$H_{10}^\psi(\mathbf{r}) = \frac{1}{\sqrt{2}}[e^{-i\psi}L_{+1}(\mathbf{r}) + e^{i\psi}L_{-1}(\mathbf{r})]$$
$$= \sqrt{2}|L_{\pm 1}(\mathbf{r})|\cos(\phi - \psi), \tag{6a}$$
$$H_{01}^\psi(\mathbf{r}) = \frac{1}{\sqrt{2}i}[e^{-i\psi}L_{+1}(\mathbf{r}) - e^{i\psi}L_{-1}(\mathbf{r})]$$
$$= \sqrt{2}|L_{\pm 1}(\mathbf{r})|\sin(\phi - \psi). \tag{6b}$$

One can thus define boson operators associated to these modes, whose relation with the LG ones is

$$\hat{a}_{10,\psi} = \frac{1}{\sqrt{2}}(e^{i\psi}\hat{a}_{+1} + e^{-i\psi}\hat{a}_{-1}), \tag{7a}$$
$$\hat{a}_{01,\psi} = \frac{i}{\sqrt{2}}(e^{i\psi}\hat{a}_{+1} - e^{-i\psi}\hat{a}_{-1}). \tag{7b}$$

These relations will be important in order to understand the properties of the system.

Finally, note that for any mode m, quadrature $\hat{X}_m^\varphi$ can be defined as

$$\hat{X}_m^\varphi = e^{-i\varphi}\hat{a}_m + e^{i\varphi}\hat{a}_m^\dagger, \tag{8}$$

and quadratures with $\varphi = 0$ and $\varphi = \pi/2$ are usually called amplitude and phase quadratures, respectively, and will be denoted by $\hat{X}$ and $\hat{Y}$, respectively.

B. Model equations of the system

Once the structure of the field inside the cavity has been described, we can proceed to describe its evolution, and to this end a Hamiltonian must be built. It has to take into account two processes: the pumping of the coherent, Gaussian, resonant laser source at frequency $2\omega_0$, and the parametric down-conversion of the pump photons into signal photons occurring in the $\chi^{(2)}$ crystal. In the interaction picture, this Hamiltonian is given by

$$\hat{H} = i\hbar(\mathcal{E}_\mathrm{p}\hat{a}_0^\dagger + \chi\hat{a}_0\hat{a}_{+1}^\dagger\hat{a}_{-1}^\dagger) + \mathrm{H.c.}, \tag{9}$$

where $\mathcal{E}_\mathrm{p}$ and χ are proportional to the injected pump amplitude and to the second-order nonlinear susceptibility of the nonlinear crystal respectively. Explicit expressions of these parameters in terms of physical quantities are given in Appendix A. We take $\mathcal{E}_\mathrm{p}$ as real; that is, we take the phase of the pump laser as the reference phase for all the other fields.

The first part of the Hamiltonian is the usual pump Hamiltonian [17], while the second part is easily justified by energy and OAM conservation: From one $2\omega_0$ photon with zero OAM, two ω_0 photons are created with opposite OAM, or vice versa. Note that this Hamiltonian is equivalent to that for the nondegenerate optical parametric oscillator (OPO in the following) considered, for example, in Refs. [18–20].

There exists one more process not taken into account in this Hamiltonian: The losses through the cavity mirrors. This is an irreversible process which cannot be described with a Hamiltonian formalism that takes into account only the cavity dynamics. However, assuming that the outer of the cavity consists of a continuum of modes in a vacuum (or coherent) state which weakly interact with the internal modes through the partially reflecting mirror, it can be incorporated into the master equation satisfied by the density operator of the system as shown for example in Ref. [21]. Moreover, the master equation can be converted into a set of stochastic (Langevin) differential equations by using a positive P representation for the density operator [22]. In our case, as is shown in [18], the equivalent set of Langevin equations is

$$\begin{aligned}
\dot{\alpha}_0 &= \mathcal{E}_\mathrm{p} - \gamma_\mathrm{p}\alpha_0 - \chi\alpha_{+1}\alpha_{-1},\\
\dot{\alpha}_0^+ &= \mathcal{E}_\mathrm{p} - \gamma_\mathrm{p}\alpha_0^+ - \chi\alpha_{+1}^+\alpha_{-1}^+,\\
\dot{\alpha}_{+1} &= -\gamma_\mathrm{s}\alpha_{+1} + \chi\alpha_0\alpha_{-1}^+ + \sqrt{\chi\alpha_0}\xi(t),\\
\dot{\alpha}_{+1}^+ &= -\gamma_\mathrm{s}\alpha_{+1}^+ + \chi\alpha_0^+\alpha_{-1} + \sqrt{\chi\alpha_0^+}\xi^+(t),\\
\dot{\alpha}_{-1} &= -\gamma_\mathrm{s}\alpha_{-1} + \chi\alpha_0\alpha_{+1}^+ + \sqrt{\chi\alpha_0}\xi^*(t),\\
\dot{\alpha}_{-1}^+ &= -\gamma_\mathrm{s}\alpha_{-1}^+ + \chi\alpha_0^+\alpha_{+1} + \sqrt{\chi\alpha_0^+}[\xi^+(t)]^*,
\end{aligned} \tag{10}$$

where α_m and α_m^+ are independent complex amplitudes, γ_p and γ_s are the decay rates of the cavity at the pump and signal frequencies, respectively (see Appendix A), and the independent complex noises ξ and ξ^+ have zero mean and nonzero correlations:

$$\langle\xi(t_1)\xi^*(t_2)\rangle = \langle\xi^+(t_1)[\xi^+(t_2)]^*\rangle = \delta(t_1 - t_2). \tag{11}$$

The equivalence between the master equation of the system and these equations must be understood in the following way:

$$\langle{:}\ f(\hat{a}_m, \hat{a}_m^\dagger)\ {:}\rangle = \langle f(\alpha_m, \alpha_m^+)\rangle_\mathrm{stochastic}; \tag{12}$$

that is, quantum expected values of normally ordered functions equal stochastic averages of the same functions changing boson operators $(\hat{a}_m,\hat{a}_m^\dagger)$ by independent complex stochastic variables (α_m,α_m^+). Note that these stochastic equations are equal in either the Ito or the Stratonovich forms (see Appendix B), and hence we interpret them as Stratonovich equations, which allow us to apply ordinary calculus.

In order to better visualize the free parameters of the model, let us define new rescaled time and amplitudes through

$$\tau = \gamma_s t,\ \beta_{\pm1} = \frac{\chi}{\sqrt{\gamma_p\gamma_s}}\alpha_{\pm1},\quad \beta_0 = \frac{\chi}{\gamma_s}\alpha_0, \tag{13}$$

and similar expressions for the conjugate fields $\alpha_{\pm1}^+$ and α_0^+. Note that as time is measured in units of γ_s^{-1}, the noises must be rescaled also as

$$\zeta_{\pm1}(\tau) = \frac{1}{\sqrt{\gamma_s}}\xi_{\pm1}(t), \tag{14}$$

and similarly for $\xi_{\pm1}^+$, if we want to preserve their statistical properties (11) in terms of the dimensionless time τ.

Finally, these changes make Langevin equations (10) read (of course, derivatives are with respect to the new dimensionless time)

$$\begin{aligned}
\dot{\beta}_0 &= \kappa(\sigma - \beta_0 - \beta_{+1}\beta_{-1}),\\
\dot{\beta}_0^+ &= \kappa(\sigma - \beta_0^+ - \beta_{+1}^+\beta_{-1}^+),\\
\dot{\beta}_{+1} &= -\beta_{+1} + \beta_0\beta_{-1}^+ + g\sqrt{\beta_0}\zeta(t),\\
\dot{\beta}_{+1}^+ &= -\beta_{+1}^+ + \beta_0^+\beta_{-1} + g\sqrt{\beta_0}\zeta^+(t),\\
\dot{\beta}_{-1} &= -\beta_{-1} + \beta_0\beta_{+1}^+ + g\sqrt{\beta_0}\zeta^*(t),\\
\dot{\beta}_{-1}^+ &= -\beta_{-1}^+ + \beta_0^+\beta_{+1} + g\sqrt{\beta_0}[\zeta^+(t)]^*,
\end{aligned} \tag{15}$$

which have only the following three dimensionless parameters:

$$\kappa = \frac{\gamma_p}{\gamma_s},\quad \sigma = \frac{\mathcal{E}_p\chi}{\gamma_p\gamma_s},\quad \text{and}\quad g = \frac{\chi}{\sqrt{\gamma_p\gamma_s}}. \tag{16}$$

Note that these equations coincide with those of the nondegenerate optical parametric oscillator, the opposite OAM modes of our model playing the role of its signal and idler modes, which in the usual OPO's configuration correspond to different frequency modes (if in addition they differ in polarization, we talk about type-II OPOs). Noncritical squeezing appears in this system both in the signal-idler-intensity difference [19] and in a joint quadrature of the signal and idler modes [20], which is useful for proving Einstein-Podolsky-Rosen quantum correlations, but not for some applications of the squeezed states (see the Introduction), which require the squeezing to be carried by a single mode of light.

Closer to our ideas is a different configuration of the OPO, namely, the frequency degenerate type-II OPO, in which the signal and idler fields correspond to two orthogonally polarized modes with the same frequency. This is an unusual but achievable configuration [23]. Just as we show in this article with opposite OAM modes, the quantum properties of this system can be analyzed in terms of a bright mode, corresponding to a superposition of the two linearly polarized signal-idler modes having an arbitrary phase difference (which is just a $\pm45^\circ$ elliptically polarized mode with an arbitrary eccentricity), and a dark mode, which corresponds to the polarization mode orthogonal to the bright one. However, this study has been carried out only when the phase difference between the signal-idler modes is locked by means of an internal wave plate [24], while here we go further by allowing for a complete indeterminacy of this phase (which is crucial for obtaining perfect squeezing according to the reasoning given in the Introduction), which needs special care when quantum noise is added.

III. CLASSICAL EMISSION: ROTATIONAL SYMMETRY BREAKING

Before analyzing the quantum properties of the system, let us examine the emission of this DOPO as predicted by classical optics. It is possible to retrieve the classical equations of the two-transverse-mode DOPO from the quantum Langevin ones (15) by setting all the noises to zero and making $\beta_m^+ = \beta_m^*$ (m refers to any mode of the problem). We are interested in finding the stationary emission; therefore, we set to zero the time derivatives of the amplitudes, arriving at

$$\begin{aligned}
\beta_0 &= \sigma - \beta_{+1}\beta_{-1},\\
\beta_{+1} &= \beta_0\beta_{-1}^*,\\
\beta_{-1} &= \beta_0\beta_{+1}^*.
\end{aligned} \tag{17}$$

Before solving these equations, let us stress that these are invariant under the following transformation:

$$\beta_{\pm1} \longrightarrow e^{\pm i\psi}\beta_{\pm1}, \tag{18}$$

and hence the phase difference between opposite OAM modes is classically undetermined.

By decomposing the amplitudes β_m into modulus and phase, it is straightforward to find the solutions of the system (17). If in addition a linear stability analysis is made, it is easy to find the following result:

(i) For $\sigma < 1$ the only stable solution is

$$\begin{aligned}
\bar{\beta}_0 &= \sigma,\\
\bar{\beta}_{\pm1} &= 0,
\end{aligned} \tag{19}$$

and hence the signal modes are off if the pump $\mathcal{E}_p$ does not exceed a threshold value $\mathcal{E}_{th} = \gamma_p\gamma_s/\chi$.

(ii) On the other hand, if $\sigma > 1$, the signal modes are switched on, and the only stable solution in this case is

$$\begin{aligned}
\bar{\beta}_0 &= 1,\\
\bar{\beta}_{\pm1} &= \rho e^{\mp i\theta},\quad \text{with}\quad \rho = \sqrt{\sigma - 1},
\end{aligned} \tag{20}$$

where, as stated previously, θ is arbitrary.

If we substitute the last result for the signal modes in the expression of the corresponding slowly varying envelope (4b), we find the generated pattern to be

$$\bar{A}_s(\mathbf{r}) = \rho[e^{-i\theta}L_{+1}(\mathbf{r}) + e^{+i\theta}L_{-1}(\mathbf{r})] = \sqrt{2}\rho H_{10}^{\theta}(\mathbf{r}), \tag{21}$$

which is a TEM_{10} mode forming an angle θ with respect to the x axis (6a) as shown in Fig. 1. Due to the arbitrariness of θ, the pattern can arise with any orientation; this reflects the rotational invariance of the system, which in turn is broken after the TEM_{10} mode generation.

In the following, we will call $H^{\theta}_{10}(\mathbf{r})$ the *bright mode* (as it is classically excited) and its orthogonal mode $H^{\theta}_{01}(\mathbf{r})$ the *dark mode* (as it is classically empty of photons), and will define the collective indices $\mathrm{b} = (10,\theta)$ and $\mathrm{d} = (01,\theta)$ to simplify the notation.

IV. QUANTUM PROPERTIES: PATTERN DIFFUSION AND NONCRITICAL SQUEEZING

A. The linearized Langevin equations

We are going to discuss the quantum properties of the down-converted field by inspection of the quantum Langevin equations (15) in the limit $\gamma_{\mathrm{p}} \gg \gamma_{\mathrm{s}}$, that is, $\kappa \gg 1$, where the pump variables can be adiabatically eliminated. We will show later (Sec. V) that all the important properties found in this limit are valid in general.

One common way of treating the adiabatic elimination of the pump consists of setting $\dot{\beta}_0 = \dot{\beta}_0^+ = 0$ in the first two equations of (15). However, this method has a problem: The initial Langevin equations are equal in either Ito or Stratonovich forms, but the new Langevin equations obtained for the signal modes do not have this property (see Appendix B). Hence, it is fair to ask within which interpretation (Ito or Stratonovich) is that procedure correct, if it is correct at all. As proved in [25] by performing the adiabatic elimination in the Fokker-Planck equation (where there are no problems of interpretation), the usual method for eliminating the pump is correct within Ito's interpretation, and hence the Stratonovich form of the stochastic equations satisfied by the signal modes only has an unexpected extra term proportional to g^2 (see Appendix B) and reads

$$\begin{aligned}
\dot{\beta}_{+1} &= -(1-g^2/4)\beta_{+1} + \beta_0\beta_{-1}^{+} + g\sqrt{\beta_0}\zeta(\tau),\\
\dot{\beta}_{+1}^{+} &= -(1-g^2/4)\beta_{+1}^{+} + \beta_0^{+}\beta_{-1} + g\sqrt{\beta_0^{+}}\zeta^{+}(\tau),\\
\dot{\beta}_{-1} &= -(1-g^2/4)\beta_{-1} + \beta_0\beta_{+1}^{+} + g\sqrt{\beta_0}\zeta^{*}(\tau),\\
\dot{\beta}_{-1}^{+} &= -(1-g^2/4)\beta_{-1}^{+} + \beta_0^{+}\beta_{+1} + g\sqrt{\beta_0^{+}}[\zeta^{+}(\tau)]^{*},
\end{aligned} \tag{22}$$

with

$$\begin{aligned}
\beta_0 &= \sigma - \beta_{+1}\beta_{+1},\\
\beta_0^{+} &= \sigma - \beta_{+1}^{+}\beta_{+1}^{+}.
\end{aligned} \tag{23}$$

In order to find analytic predictions from these equations, we assume well above threshold operating conditions, where classical emission dominates, thus allowing for a linearization procedure. The correct way to perform this was described in [5,26] and relies on the smallness of the g parameter (see Appendix A). In particular, making a perturbative expansion of the amplitudes in terms of this parameter, it is possible to show that the classical equations are recovered as the g^0 order of the expansion in Eqs. (22), while the linear quantum correction appears in the g^1 order (note that the noise term is already of order g^1).

Hence, the usual linearization procedure begins by writing the amplitudes as $\beta_m = \bar{\beta}_m + \delta\beta_m$ and $\beta_m^{+} = \bar{\beta}_m^{*} + \delta\beta_m^{+}$ and treating the fluctuations as order-g perturbations. However, as stated in the Introduction, in the system we are dealing with, we expect that quantum noise rotates the generated TEM_{10} mode, and hence fluctuations of the fields in an arbitrary direction of phase space could not be small (i.e., order g). Nevertheless, Eqs. (22) can be linearized if the amplitudes are expanded as

$$\begin{aligned}
\beta_{\pm1}(\tau) &= [\rho + b_{\pm1}(\tau)]e^{\mp i\theta(\tau)},\\
\beta_{\pm1}^{+}(\tau) &= [\rho + b_{\pm1}^{+}(\tau)]e^{\pm i\theta(\tau)},
\end{aligned} \tag{24}$$

because as we will prove $\theta(\tau)$ carries the larger part of the fluctuations, while the b's and $\dot{\theta}$ remain as order-g quantities. In addition, expanding the fields in this way allows us to track the evolution of the classical pattern's orientation, as we take θ as an explicit quantum variable. Then, writing Eqs. (22) up to order g, we arrive at the following linear system (arriving to this expression is not as straightforward as it might seem; see Appendix C):

$$-2i\rho\mathbf{w}_0\dot{\theta} + \dot{\mathbf{b}} = \mathcal{L}\mathbf{b} + g\boldsymbol{\zeta}(\tau), \tag{25}$$

with

$$\mathbf{b} = \begin{pmatrix} b_{+1}\\ b_{+1}^{+}\\ b_{-1}\\ b_{-1}^{+}\end{pmatrix} \qquad \boldsymbol{\zeta}(\tau) = \begin{pmatrix} \zeta(\tau)\\ \zeta^{+}(\tau)\\ \zeta^{*}(\tau)\\ [\zeta^{+}(\tau)]^{*}\end{pmatrix}, \tag{26}$$

and where $\mathcal{L}$ is a real, symmetric matrix given by

$$\mathcal{L} = -\begin{pmatrix} \sigma & 0 & \sigma-1 & -1\\ 0 & \sigma & -1 & \sigma-1\\ \sigma-1 & -1 & \sigma & 0\\ -1 & \sigma-1 & 0 & \sigma\end{pmatrix}, \tag{27}$$

with the following eigensystem:

$$\begin{aligned}
\lambda_0 &= 0, \quad & \mathbf{w}_0 &= \tfrac{1}{2}\mathrm{col}(1,-1,-1,1),\\
\lambda_1 &= -2, \quad & \mathbf{w}_1 &= \tfrac{1}{2}\mathrm{col}(1,1,-1,-1),\\
\lambda_2 &= -2(\sigma-1), \quad & \mathbf{w}_2 &= \tfrac{1}{2}\mathrm{col}(1,1,1,1),\\
\lambda_3 &= -2\sigma, \quad & \mathbf{w}_3 &= \tfrac{1}{2}\mathrm{col}(1,-1,1,-1).
\end{aligned} \tag{28}$$

Defining the projections $c_m(\tau) = \mathbf{w}_m \cdot \mathbf{b}(\tau)$, and projecting the linear system (25) onto these eigenmodes, we find the following set of decoupled linear equations (c_0 is set to zero, as otherwise it would just entail a redefinition of θ):

$$\dot{\theta} = \frac{g}{2\rho}\eta_0(\tau), \tag{29a}$$

$$\dot{c}_1 = -2c_1 + ig\eta_1(\tau), \tag{29b}$$

$$\dot{c}_2 = -2(\sigma-1)c_2 + g\eta_2(\tau), \tag{29c}$$

$$\dot{c}_3 = -2\sigma c_3 + g\eta_3(\tau), \tag{29d}$$

where the following real noises have been defined:

$$\begin{aligned}
\eta_0(\tau) &= i\mathbf{w}_0\cdot\boldsymbol{\zeta}(\tau) = \mathrm{Im}\{\zeta^{+}(\tau) - \zeta(\tau)\},\\
\eta_1(\tau) &= -i\mathbf{w}_1\cdot\boldsymbol{\zeta}(\tau) = \mathrm{Im}\{\zeta^{+}(\tau) + \zeta(\tau)\},\\
\eta_2(\tau) &= \mathbf{w}_2\cdot\boldsymbol{\zeta}(\tau) = \mathrm{Re}\{\zeta(\tau) + \zeta^{+}(\tau)\},\\
\eta_3(\tau) &= \mathbf{w}_3\cdot\boldsymbol{\zeta}(\tau) = \mathrm{Re}\{\zeta(\tau) - \zeta^{+}(\tau)\},
\end{aligned} \tag{30}$$

which have zero mean and nonzero correlations,

$$\langle\eta_m(\tau_1)\eta_n(\tau_2)\rangle = \delta_{mn}\delta(\tau_1-\tau_2). \tag{31}$$

Note finally that the solutions for the projections c_j will be of order g (see Appendix D), and hence so will be the b's (note that this is not the case for θ, whose initial value is completely

arbitrary, although its variation $\dot{\theta}$ is indeed of order g). This is consistent with the initial assumptions about the orders in g of the involved quantities.

B. Quantum diffusion of the classical pattern

The first quantum effect that we are going to show concerns the orientation of the classically generated mode. Equation (29a) defines a *Wiener process* for θ, thus showing that the orientation of this bright mode diffuses with time ruled by quantum noise.

How fast this diffusion is can be measured by evaluating the variance of θ. Using the statistical properties of noise (31), it is straightforward to obtain the following result:

$$V_\theta(\tau) = \langle \delta\theta^2(\tau)\rangle = D\tau, \tag{32}$$

where $D = d/(\sigma - 1)$, with

$$d = g^2/4 = \chi^2/4\gamma_\mathrm{p}\gamma_\mathrm{s}. \tag{33}$$

In (32) the notation $\delta A = A - \langle A\rangle$ has been used.

Equation (32) shows that the delocalization of the pattern's orientation increases as time passes, though for typical system parameters (see Appendix A) one finds $d \simeq 4\times 10^{-13}$, and hence the rotation of the pattern will be fast only when working very close to threshold [27].

C. Squeezing properties of the two-transverse-mode DOPO

1. Definition and criteria for squeezing

In the Introduction we defined squeezed light as that having some quadrature fluctuating below the vacuum level. Hence, in order to find out whether a light beam is in a squeezed state or not, one has to measure its *quadrature fluctuations* and then compare them with the value set by the vacuum state. The question then is: What quantity accounts for quadrature fluctuations of a light beam? Of course, in the case of a single mode of light this quantity can be directly the uncertainty of the quadrature. However, outside the cavity there exists a continuum of modes, and the quantity accounting for these fluctuations has to be adapted to what can be most easily observed in an experiment.

As was first shown in [4], the quantity accounting for fluctuations of quadrature $\hat{X}_m^\varphi$ outside the cavity (m refers to any signal spatial mode of our two-transverse-mode DOPO) is

$$V^\mathrm{out}\big(\omega;\hat{X}_m^\varphi\big) = 1 + S_m^\varphi(\omega), \tag{34}$$

with

$$S_m^\varphi(\omega) = \frac{2}{g^2}\int_{-\infty}^{+\infty} d\bar{\tau}\,\big\langle :\delta\hat{X}_m^\varphi(\tau)\delta\hat{X}_m^\varphi(\tau+\bar{\tau}):\big\rangle e^{-i\omega\bar{\tau}}, \tag{35}$$

where the factor g^{-2} appears after including our rescaled variables (13).

We will call V^out the *noise spectrum* and $S_m^\varphi(\omega)$ the *squeezing spectrum*. Frequency ω is usually called *noise frequency*, and it must not be confused with the optical frequency. In fact, noise frequency ω has contributions of every pair of modes lying in opposite sidebands around the optical frequency $\omega_0+\omega$, where ω_0 is the carrier frequency of the detected beam (do not miss that in our case this frequency is measured in units of γ_s).

V^out can be measured via a balanced homodyne-detection experiment: A coherent, intense field (local oscillator field) prepared in mode m and with a phase φ is mixed with the beam exiting the DOPO in a 50-50 beam splitter; it is easy to show that the operator associated to the intensity difference between the two output ports of the beam splitter is proportional to the quadrature $\hat{X}_m^{\varphi,\mathrm{out}}$ of the beam exiting the DOPO. Hence, the normalized correlation spectrum of the intensity difference (which can be measured with a simple spectrum analyzer) coincides with expression (34). Factor 2 in (35) comes from the relation between the intracavity and the output modes when the input modes (the pump laser and the outer modes) are coherent; this factor is $2\gamma_\mathrm{s}$ when time (frequency) is not normalized to γ_s^{-1} (γ_s).

In the preceding expression for the squeezing spectrum, it is assumed that the emission of the DOPO reaches a stationary state (i.e., the correlation function of $\delta\hat{X}_m^\varphi$ at two different times τ and $\tau+\bar{\tau}$ depends only on the time difference $|\bar{\tau}|$) and that the observation time, say T, is large as compared with the coherence time of $\delta\hat{X}_m^\varphi$. In the two-transverse-mode DOPO there exists an undamped quantity excited by quantum noise, θ, and hence, any quantity with explicit dependence on it will not arrive at a stationary state. Thus, under some circumstances we will need the expression of the squeezing spectrum measured when the field is not stationary, which was derived in [28]. In that reference it is shown that when the measurement extends during a time interval T (normalized to γ_s^{-1} in our expressions) the squeezing spectrum reads

$$S_m^\varphi(\omega) = \frac{2}{g^2T}\int_0^T\int_0^T d\tau d\tau'\big\langle :\delta\hat{X}_m^\varphi(\tau)\delta\hat{X}_m^\varphi(\tau'):\big\rangle \times\cos[\omega(\tau-\tau')], \tag{36}$$

which obviously reduces to (35) if the emission is stationary.

For the vacuum state $V^\mathrm{out}=1$; hence, if $V^\mathrm{out}(\tilde{\omega};\hat{X}_m^\varphi)<1$ for some frequency $\tilde{\omega}$, we can say that the detected light is in a squeezed state for mode m at noise frequency $\tilde{\omega}$.

Finally, let us stress that we will evaluate quantum correlations as those involved in (36) via stochastic correlations, as allowed by property (12). Hence, in the following we will change operators by their equivalent stochastic variables within the positive P representation in all the preceding definitions, and their associated normally ordered correlations by the corresponding stochastic correlations.

2. Independent quadratures and noncritical squeezing

A first step toward analyzing the squeezing properties of the field within the framework presented previously is identifying a set of independent quadratures. This is easy in our case, as the eigenmodes $\mathbf{w}_m$ give us a set of quadratures with well-defined squeezing properties. In particular, from (24), (7), and (8), it is easy to find the following relations:

$$\begin{aligned} X_\mathrm{b}(\tau) &= 2\sqrt{2}\rho + \sqrt{2}c_2(\tau),\\ Y_\mathrm{b}(\tau) &= -i\sqrt{2}c_3(\tau),\\ X_\mathrm{d}(\tau) &= i\sqrt{2}c_0(\tau),\\ Y_\mathrm{d}(\tau) &= \sqrt{2}c_1(\tau), \end{aligned} \tag{37}$$

where (X_b, Y_b) and (X_d, Y_d) are the amplitude and phase quadratures of the bright and dark modes, $H^{\theta}_{10}(\mathbf{r})$ and $H^{\theta}_{01}(\mathbf{r})$, respectively.

The evolution of these quadratures can be found from the equations satisfied by the projections (29), which are solved in Appendix D (remember that $c_0 = 0$). In particular, there we show that after some time these projections reach a stationary state, and hence we can evaluate the noise spectrum of the quadratures by using the stationary expression for the squeezing spectrum (35). Using the results found in Appendix D for the correlation spectrum of the projections (D7), it is straightforward to find the following results:

$$V^{\text{out}}(\omega; X_b) = 1 + \frac{1}{(\sigma - 1)^2 + \omega^2/4}, \tag{38a}$$

$$V^{\text{out}}(\omega; Y_b) = 1 - \frac{1}{\sigma^2 + \omega^2/4}, \tag{38b}$$

$$V^{\text{out}}(\omega; X_d) = 1, \tag{38c}$$

$$V^{\text{out}}(\omega; Y_d) = 1 - \frac{1}{1 + \omega^2/4}. \tag{38d}$$

We see that the quadratures of the bright mode have the same behavior as those of the single-mode DOPO: The phase quadrature Y_b is perfectly squeezed ($V^{\text{out}} = 0$) at zero noise frequency ($\omega = 0$) only at the bifurcation ($\sigma = 1$).

On the other hand, the dark mode has perfect squeezing in its phase quadrature Y_d at zero noise frequency. What is interesting is that this result is independent of the distance from threshold, and thus, it is a noncritical phenomenon.

This result was first shown in [12], and we can understand it by following the reasoning given in the Introduction: As the orientation θ of the classically excited pattern is undetermined in the long-time limit, its OAM must be fully determined at low noise frequencies. On the other hand, the OAM of the bright mode $H^{\theta}_{10}(\mathbf{r})$ is nothing but its $\pi/2$ phase shifted orthogonal HG mode; that is, $-i\,\partial_{\phi} H^{\theta}_{10}(\mathbf{r}) = i\,H^{\theta}_{01}(\mathbf{r})$, which, if used as a local oscillator in an homodyne detection experiment, would lead to the observation of the Y_d quadrature fluctuations.

3. *On canonical pairs and noise transfer*

Although all the results we have discussed up to now were expected to occur after the arguments given in the Introduction, a strange unexpected result has appeared in (38): The quadratures of the dark mode seem to violate the uncertainty principle as $V^{\text{out}}(\omega = 0; X_d)V^{\text{out}}(\omega = 0; Y_d) = 0$.

Moreover, the noise spectrum of an arbitrary quadrature of the dark mode, which can be written in terms of its amplitude and phase quadratures as $X^{\varphi}_d = X_d \cos\varphi + Y_d \sin\varphi$, is

$$V^{\text{out}}\left(\omega; X^{\varphi}_d\right) = 1 - \frac{\sin^2\varphi}{1 + \omega^2/4}, \tag{39}$$

which shows that all the quadratures of the dark mode (except its amplitude quadrature) are squeezed. Thus, two orthogonal quadratures cannot form a canonical pair as they satisfy the relation

$$V^{\text{out}}\left(\omega; X^{\varphi}_d\right) V^{\text{out}}\left(\omega; X^{\varphi+\pi/2}_d\right) < 1, \tag{40}$$

in clear violation of the uncertainty principle.

The natural question now is: Where does the excess of noise go if it is not transferred from one quadrature to its orthogonal one? The answer is that it goes to the pattern orientation, which is actually fully undetermined in the long term, as we showed in Eq. (32). This section is devoted to proving this statement.

In particular, we will prove that two orthogonal quadratures of the dark mode do not form a canonical pair, while the orientation θ is the canonical pair of all the squeezed quadratures. One way to prove this would be to evaluate the commutator between the quantum operators involved. However, θ is half the phase difference between the opposite OAM modes $\beta_{\pm 1}$, whose associated operator has a very difficult expression [29], making the calculation of the needed commutators quite hard. Nevertheless, in [15] we developed a simple proof based on classical field methods, and this is the one we present here.

A usual approach one uses to move from classical to quantum optics is to change the classical normal variables for each mode of the field, β_m and β^*_m, by boson operators $\hat{a}_m$ and $\hat{a}^{\dagger}_m$, satisfying commutation relations

$$[\hat{a}_m, \hat{a}^{\dagger}_m] = i\{\beta_m, \beta^*_m\}, \tag{41}$$

where $\{f, h\}$ denotes the *Poisson bracket* between two functions $f(\beta_m, \beta^*_m)$ and $h(\beta_m, \beta^*_m)$, defined as

$$\{f, h\} = \frac{1}{i}\sum_m \frac{\partial f}{\partial \beta_m}\frac{\partial h}{\partial \beta^*_m} - \frac{\partial f}{\partial \beta^*_m}\frac{\partial h}{\partial \beta_m}. \tag{42}$$

As an example, the Poisson bracket of two monomode orthogonal quadratures $X_m = \beta_m + \beta^*_m$ and $Y_m = -i(\beta_m - \beta^*_m)$ is found to be

$$\{X_m, Y_m\} = 2. \tag{43}$$

In general, two phase space functions $f(\beta_m, \beta^*_m)$ and $h(\beta_m, \beta^*_m)$ are said to form a canonical pair if their Poisson bracket is of the form

$$\{f, h\} = C, \tag{44}$$

with C a real number.

In our case, the functions we are interested in are the classical counterparts of the dark-mode quadratures, which using (7b) with $\psi = \theta$ are written as

$$X^{\varphi}_d = \frac{i}{\sqrt{2}}[e^{-i\varphi}(e^{i\theta}\beta_{+1} - e^{-i\theta}\beta_{-1})] + \text{c.c.}, \tag{45}$$

with the orientation given by

$$\theta = \frac{1}{2i}\ln\left[\frac{\beta^*_{+1}\beta_{-1}}{\sqrt{\beta^*_{+1}\beta_{+1}}\sqrt{\beta^*_{-1}\beta_{-1}}}\right]. \tag{46}$$

Now using the definition of the Poisson brackets with $m = \pm 1$ and after some algebra, it is possible to show that

$$\left\{X^{\varphi}_d, X^{\varphi+\pi/2}_d\right\} = \frac{|\beta_{-1}| - |\beta_{+1}|}{2|\beta_{+1}||\beta_{-1}|}, \tag{47}$$

and

$$\left\{X^{\varphi}_d, \theta\right\} = \frac{i(|\beta_{+1}| + |\beta_{-1}|)(e^{i\varphi}|\beta_{-1}| - e^{-i\varphi}|\beta_{-1}|)}{4\sqrt{2}|\beta_{+1}|^{3/2}|\beta_{-1}|^{3/2}}, \tag{48}$$

with $|\beta_m| = \sqrt{\beta^*_m\beta_m}$.

On the other hand, in the two-transverse-mode DOPO, the number of photons with opposite OAM is sensibly equal, that is, $|\beta_{+1}| \approx |\beta_{-1}|$; hence, the dominant term of the previous brackets will be that with $|\beta_{+1}| = |\beta_{-1}| = \rho$, and thus

$$\left\{X_{\mathrm{d}}^{\varphi}, X_{\mathrm{d}}^{\varphi+\pi/2}\right\} \approx 0 \tag{49}$$

and

$$\left\{X_{\mathrm{d}}^{\varphi}, \theta\right\} \approx -\frac{\sin\varphi}{\sqrt{2}\rho}. \tag{50}$$

Comparing these with (44), we find that this is a confirmation of what we expected: two orthogonal dark quadratures X_{d}^{φ} and $X_{\mathrm{d}}^{\varphi+\pi/2}$ do not form a canonical pair (moreover, they commute), while X_{d}^{φ} and θ do. This can be seen as an indirect proof of the same conclusion for the corresponding operators.

4. Homodyne detection with a fixed local oscillator

So far we have considered the situation in which one is able to detect independently the bright and dark modes. However, as shown by Eq. (29a), these modes are rotating randomly, which means that a local oscillator field following that random rotation should be used in order to detect them separately. This might be a really complicated, if not impossible, task, so we analyze now the more realistic situation in which the local oscillator is matched to the orthogonal orientation of the emerging pattern only at some initial time, remaining then with the same orientation during the observation time. We will show that even in this case, and as the rotation of the modes is quite slow (32), large levels of noise reduction can be obtained.

Without loss of generality, we suppose that the bright mode emerges from the resonator at some initial time $\tau = 0$ oriented within the x axis; that is, $\theta(0) = 0$. Hence, by using a TEM_{01} local oscillator with a phase φ, the quadrature X_{01}^{φ} of a fixed $H_{01}(\mathbf{r})$ mode (the initially dark mode) will be measured. In terms of the Laguerre-Gauss modes, the amplitude β_{01} of the this mode is given by (7b), with $\psi = 0$. Then, by using the expansion (24) of the amplitudes β_m as functions of the fluctuations b_m and the orientation θ, quadrature X_{01}^{φ} of this mode can be rewritten as

$$\begin{aligned} X_{01}^{\varphi} = {} & 2\sqrt{2}\rho\cos\varphi\sin\theta + \sqrt{2}c_2\cos\varphi\sin\theta \\ & + \sqrt{2}c_1\sin\varphi\cos\theta - i\sqrt{2}c_3\sin\varphi\sin\theta. \end{aligned} \tag{51}$$

Hence, the two-time correlation function of X_{01}^{φ} yields [note that (29) shows that c_1, c_2, c_3, $\sin\theta$, and $\cos\theta$ are uncorrelated]

$$\begin{aligned} \left\langle X_{01}^{\varphi}(\tau_1) X_{01}^{\varphi}(\tau_2)\right\rangle = {} & 2\cos^2\varphi S(\tau_1,\tau_2)[4\rho^2 + C_2(\tau_1,\tau_2)] \\ & + 2\sin^2\varphi[C_1(\tau_1,\tau_2)C(\tau_1,\tau_2) \\ & - C_3(\tau_1,\tau_2)S(\tau_1,\tau_2)], \end{aligned} \tag{52}$$

with

$$\begin{aligned} S(\tau_1,\tau_2) &= \langle\sin\theta(\tau_1)\sin\theta(\tau_2)\rangle, \\ C(\tau_1,\tau_2) &= \langle\cos\theta(\tau_1)\cos\theta(\tau_2)\rangle, \\ C_m(\tau_1,\tau_2) &= \langle c_m(\tau_1)c_m(\tau_2)\rangle. \end{aligned} \tag{53}$$

As shown in Appendices D and E, the latter correlation functions can be evaluated by using the linear evolution equations of the projections c_m and θ [see Eqs. (D6), (E4), and (E5)]; then from (52) the squeezing spectrum of X_{01}^{φ} can be found by using the general expression (36), as in this case the stationary expression (35) cannot be used because $S(\tau_1,\tau_2)$ and $C(\tau_1,\tau_2)$ do not reach a stationary state.

Although the general expression for $S_{01}^{\varphi}(\omega)$ is too lengthy to be written here, a more compact approximated expression can be found in the limit of small d, leading to the following expression for the noise spectrum

$$V^{\mathrm{out}}\left(\omega; X_{01}^{\varphi}\right) = 1 + S_{01}^{0}(\omega)\cos^2\varphi + S_{01}^{\pi/2}(\omega)\sin^2\varphi, \tag{54}$$

with

$$S_{01}^{0} = \frac{8}{\omega^2}(1 - \mathrm{sinc}\,\omega T) - \frac{4dT}{\omega^2(\sigma-1)}\frac{6(\sigma-1)^2+\omega^2}{4(\sigma-1)^2+\omega^2} \tag{55}$$

and

$$\begin{aligned} S_{01}^{\pi/2} = {} & \frac{8-2\omega^2}{T(4+\omega^2)^2} - \frac{4}{4+\omega^2} \\ & + \frac{8dT[2(\sigma^2+1)+\omega^2]}{(\sigma-1)(4+\omega^2)(4\sigma^2+\omega^2)}, \end{aligned} \tag{56}$$

where $\mathrm{sinc}\,x = \sin(x)/x$. In the following we will fix σ to $\sqrt{2}$ (pump power twice above threshold), as the results are almost independent of its value as far as it is far enough from threshold. Hence, the free parameters will be the detection parameters T, ω, and φ, and the diffusion d, which depends on the system parameters.

In this section, the results for V^{out} are presented in dB units, defined through the relation $V^{\mathrm{out}}[\mathrm{dB}] = 10\log_{10} V^{\mathrm{out}}$ [hence, e.g., -10 dB and $-\infty$ dB correspond to 90% of noise reduction ($V^{\mathrm{out}} = 0.1$) and complete noise reduction ($V^{\mathrm{out}} = 0$) respectively].

From expression (54) we see that the maximum level of squeezing is obtained at $\omega = 0$ [see also Fig. 3(a)] and when the phase of the local oscillator is tuned exactly to $\pi/2$. In Fig. 2 we show the noise spectrum (54) for these parameters as a function of the detection time T for three different values of d. We see that in all cases there exists an optimum detection time for which squeezing is maximum. Minimizing Eq. (54) with $\omega = 0$ and $\varphi = \pi/2$ with respect to T, it is straightforward to find that this optimum detection time is given by

$$T_{\mathrm{opt}} = \sqrt{\frac{\sigma^2(\sigma-1)}{d(\sigma^2+1)}}, \tag{57}$$

with an associated noise spectrum $V_{\mathrm{opt}}^{\mathrm{out}} = 1/T_{\mathrm{opt}}$ (shown in the inset of Fig. 2 as function of d).

These results show that large levels of noise reduction are obtained for the phase quadrature of the fixed TEM_{01} mode, even for values of the diffusion parameter d as large as 10^{-6} (remember that 10^{-13} is a more realistic value). However, in real experiments it is not possible to ensure that $\varphi = 90^{\circ}$ with an uncertainty below approximately 1.5° [2,3], and hence we proceed now to investigate the level of noise reduction predicted by (54) when the local oscillator phase is different from $\varphi = 90^{\circ}$.

Of course, when $\varphi \neq 90^{\circ}$ the noise frequency with maximum squeezing is no longer $\omega = 0$, as in this case the infinite fluctuations of S_{01}^{0} at zero noise frequency, due to the rotation noise, enter the noise spectrum [see Fig. 3(a)]. By minimizing V^{out} with respect to ω and T for different values of φ and d, it is possible to show that the optimum value of the detection time is almost independent of φ for small deviations of this

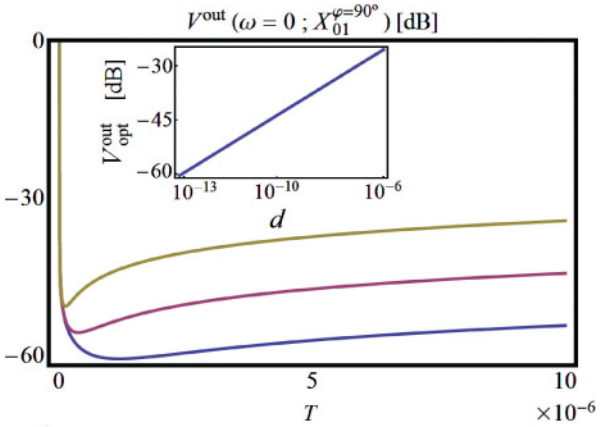

FIG. 2. (Color online) Zero-frequency noise spectrum of the phase quadrature corresponding to a fixed TEM_{01} mode as a function of the detection time T. Three different values of d are considered (10^{-11}, 10^{-12}, and 10^{-13} from top to bottom). (Inset) The spectrum at zero noise frequency, but evaluated at the optimum detection time $T_{\rm opt}$ and as a function of d (note that the d axis is in logarithmic scale). As mentioned in the text, $\sigma=\sqrt{2}$.

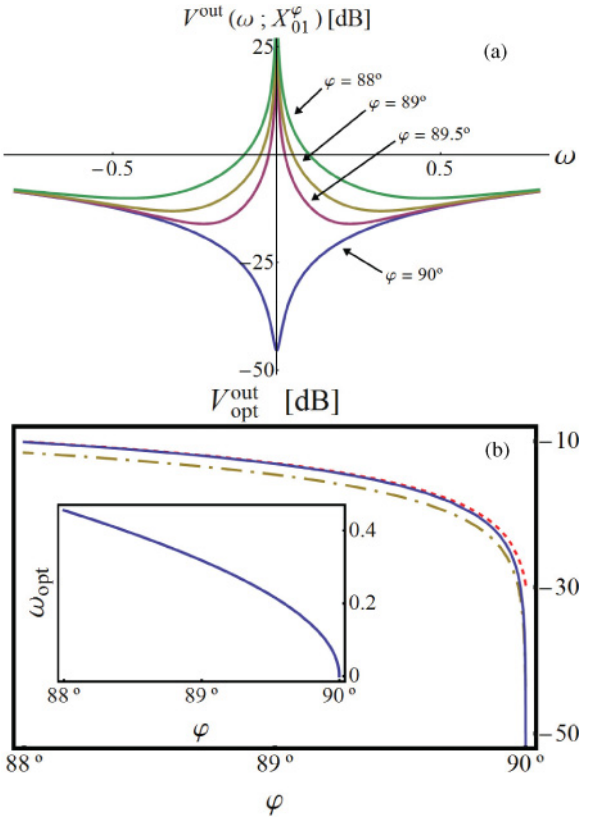

FIG. 3. (Color online) (a) Noise spectrum of the fixed TEM_{01} mode as a function of the noise frequency ω and for four different values of the local oscillator phase ($\varphi=88^\circ$, 89°, 89.5°, and 90° from top to bottom curves). It can be appreciated how the infinite fluctuations of S_{01}^0 at zero noise frequency enter in the spectrum for any $\varphi\neq 90$. The rest of parameters are $\sigma=\sqrt{2}$, $d=10^{-10}$, and $T=T_{\rm opt}$, but the same behavior appears for any election of the parameters. (b) Noise spectrum of the fixed TEM_{01} mode evaluated for the optimum parameters $\omega_{\rm opt}$ and $T_{\rm opt}$ as a function of φ ($d=10^{-13}$ for the blue solid curve and 10^{-6} for the red dashed one, having both $\sigma=\sqrt{2}$). In addition, it is plotted the analogous curve for the single-mode DOPO (gold, dashed-dotted curve). (Inset) Dependence of the optimum frequency $\omega_{\rm opt}$ on the phase of the local oscillator φ.

from 90°, and hence it is still given to a good approximation by (57), though in this case this minimum is less pronounced than in the $\varphi=90^\circ$ case shown in Fig. 2 (i.e., the curve is almost horizontal around $T_{\rm opt}$). On the other hand, the optimum noise frequency $\omega_{\rm opt}$ is independent of d and depends on φ as shown in the inset of Fig. 3(b).

As for the squeezing level, in Fig. 3(b) we show the noise spectrum evaluated at $T_{\rm opt}$ and $\omega_{\rm opt}$ as a function of φ for two different values of the diffusion d. Together with these curves, we have plotted the noise spectrum of the single-mode DOPO [30] evaluated for its optimum parameters (in this case it is optimized with respect to σ and ω) as a function of φ. We see that the noise reduction is independent of d as φ is taken apart from 90°. On the other hand, the squeezing level is similar to that of the single-mode DOPO, as the maximum difference between them is 1.5 dB (a factor 1.4 in the noise spectrum) in favor of the single-mode DOPO, with the advantage that in the two-transverse-mode DOPO this level is independent of the distance from threshold.

Therefore, we see that the phenomenon of noncritical squeezing through spontaneous rotational symmetry breaking could be observed in the two-transverse-mode DOPO without the need of following the random rotation of the generated pattern, which makes its experimental realization feasible with current available technology.

V. BEYOND THE CONSIDERED APPROXIMATIONS

A. Beyond the adiabatic elimination of the pump

The first assumption made in the search for the quantum properties of the system was that $\gamma_{\rm p}\gg\gamma_{\rm s}$, a limit that allowed the adiabatic elimination of the pump field. Now we are going to show analytically that the phenomenon of squeezing induced by spontaneous rotational symmetry breaking is still present even without this assumption, but still working in the domain where linearization is correct.

The way to show this is quite simple; starting from the complete equations (15), we expand the amplitudes β_m around the classical stationary solution (20) as we made in (24), but adding now a similar expression for the pump amplitudes: $\beta_0=1+b_0$ and $\beta_0^+=1+b_0^+$ (note that for the pump modes the b's are directly small as the phase of this mode is locked to that of the injection $\mathcal{E}_{\rm p}$). Then, linearizing these equations for the fluctuations and noises, we arrive at a linear system formally equal to (25), but with

$$\mathbf{b}=\begin{pmatrix} b_0\\ b_0^+\\ b_{+1}\\ b_{+1}^+\\ b_{-1}\\ b_{-1}^+\end{pmatrix},\qquad \boldsymbol{\zeta}=\begin{pmatrix} 0\\ 0\\ \zeta(\tau)\\ \zeta^+(\tau)\\ \zeta^*(\tau)\\ [\zeta^+(\tau)]^*\end{pmatrix}, \tag{58}$$

and a linear matrix

$$\mathcal{L} = \begin{pmatrix} -\kappa & 0 & -\rho & 0 & -\rho & 0 \\ 0 & -\kappa & 0 & -\rho & 0 & -\rho \\ \rho & 0 & -1 & 0 & 0 & 1 \\ 0 & \rho & 0 & -1 & 1 & 0 \\ \rho & 0 & 0 & 1 & -1 & 0 \\ 0 & \rho & 1 & 0 & 0 & -1 \end{pmatrix}. \tag{59}$$

Although in this case $\mathcal{L}$ is not Hermitian, it can be seen that it possess a biorthonormal basis [31] and, in particular, the following two vectors are present in its eigensystem: $\mathbf{w}_0' = \frac{1}{2}\mathrm{col}(0,0,1,-1,-1,1)$ and $\mathbf{w}_1' = \frac{1}{2}\mathrm{col}(0,0,1,1,-1,-1)$, with corresponding eigenvalues $\lambda_0' = 0$ and $\lambda_1' = -2$. These eigenvectors have null projection onto the pump subspace and coincide with $\mathbf{w}_0$ and $\mathbf{w}_1$ in what concerns to the signal subspace (28). Hence, all the properties derived from these vectors are still present without any change. In particular, as they account for the diffusion of θ and the squeezing properties of the dark mode, we can conclude that these properties are still present when working out of the limit $\gamma_p \gg \gamma_s$.

B. Numerical simulation of the nonlinear equations

In this section we will show that the diffusion of the orientation and the associated noncritical squeezing of the dark mode, which have been found by linearizing the Langevin equations, are also present when we consider the full nonlinear problem. To do so, we will solve numerically the complete stochastic equations (15) using the semi-implicit algorithm developed by Drummond and Mortimer in [32].

The details of the numerical simulation are explained in Appendix F. Here we just want to point out that the important parameters of the simulation are the step size $\Delta\tau$ used to arrive from $\tau = 0$ to the final integration time τ_{end}, and the number of stochastic trajectories, say Σ, that are used to evaluate stochastic averages. The initial conditions $\beta_m(0)$ are not important as the results in the stationary limit are independent of them. The system parameters that have been chosen for the simulation are $\sigma = \sqrt{2}$, $\kappa = 1$ (to show also numerically that the adiabatic elimination has nothing to do with the phenomenon), and $g = 10^{-3}$. We have not chosen a smaller value for g (like 10^{-6}, as followed from the physical parameters considered in Appendix A) because such a small number can make the simulation fail; nevertheless, all the results we are going to show should be independent of g and σ, and we have also tested that the same results are obtained for other values of these.

It is also important to note that we have defined a general quadrature of the rotating dark mode as [directly from (7b) with $\beta = \theta$]

$$X_{\mathrm{d}}^{\varphi} = \frac{i}{\sqrt{2}}[e^{-i\varphi}(e^{i\theta}\beta_{+1} - e^{-i\theta}\beta_{-1})] - \frac{i}{\sqrt{2}}[e^{i\varphi}(e^{-i\theta}\beta_{+1}^{+} - e^{i\theta}\beta_{-1}^{+})], \tag{60}$$

with θ defined within the positive P representation through

$$e^{2i\theta} = \frac{\beta_{-1}\beta_{+1}^{+}}{|\beta_{-1}||\beta_{+1}^{+}|}. \tag{61}$$

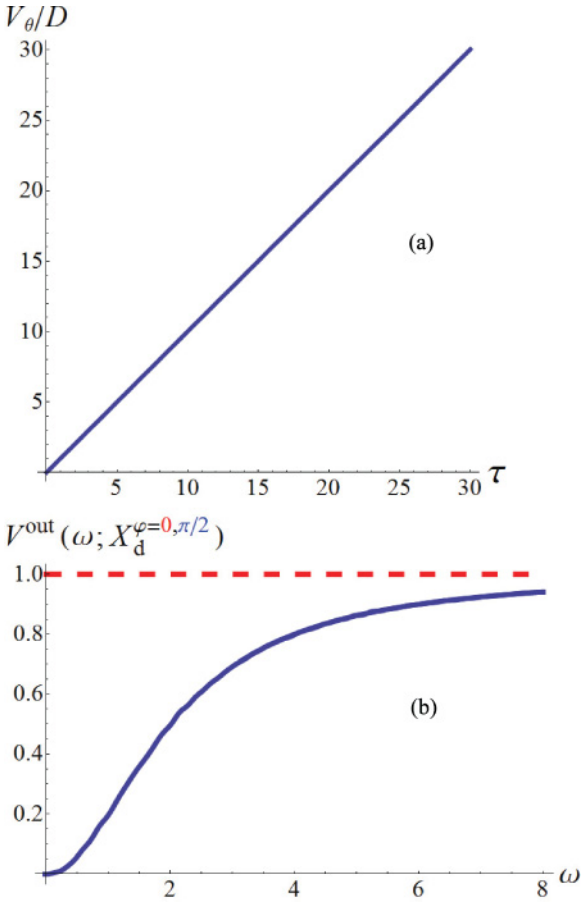

FIG. 4. (Color online) (a) Evolution of the variance of the orientation θ given by the numerical simulation. It has been divided by the slope D predicted by the linearized theory (32), so the straight line obtained is in perfect agreement with this linear result. Quantitatively, a linear regression analysis shows that the slope obtained by the data is 0.999 85, with standard error 7×10^{-5}. (b) Noise spectrum of the amplitude (red dashed curve) and phase (blue solid curve) quadratures of the dark mode as obtained by the numerical simulation. The results are in perfect agreement with the ones predicted by the linearized theory (38). In particular, a nonlinear regression analysis of the numerical data respect to the function $(\omega/2)^2/[b + a(\omega/2)^2]$ shows that $(a,b) = (0.9996, 1.0071)$ are the best fit parameters having standard errors $(1 \times 10^{-4}, 4 \times 10^{-4})$, which is in good agreement with the values $(a,b) = (1,1)$ predicted by (38). Note finally that the small oscillations of the blue solid line would disappear by increasing the number of stochastic trajectories Σ.

Now let us show the results evaluated for the following simulation parameters: $\Delta\tau = 3 \times 10^{-3}$, $\tau_{\mathrm{end}} = 30$, and $\Sigma = 7.5 \times 10^6$. This simulation has been compared with other ones having different values of these parameters to ensure convergence.

In Fig. 4(a) we show the variance of θ as a function of time. The result has been normalized to D, so that the linear result (32) predicts a straight line forming 45° with respect to the time axis. It can be appreciated that this is indeed what the simulation shows.

In Fig. 4(b), we show the numerical results for the noise spectrum associated to the quadratures of the dark mode. Only times above $\tau = 10$ have been considered in the correlation

function to ensure being in the stationary limit. Again, the results shown in Fig. 4(b) are in perfect agreement with the linear predictions (38c) and (38d).

These results show that the phenomenon of noncritically squeezed light via spontaneous rotational symmetry breaking is not a product of the linearization.

VI. CONCLUSIONS

In conclusion, we have developed in detail the quantum theory of the two-transverse-mode DOPO introduced in [12]. We have studied some important features not considered in that reference:

(i) When pumping with a Gaussian mode a rotationally symmetric DOPO properly tuned to the first family of transverse modes at the signal frequency, classical emission takes place in a TEM_{10} mode with an arbitrary orientation in the transverse plane. Hence, once the threshold is crossed, the rotational symmetry is spontaneously broken, and we can talk about a bright mode (the generated one which breaks the symmetry) and a dark mode (the mode orthogonal to the generated one).

(ii) The symmetry breaking reflects in the appearance of a Goldstone mode in the matrix governing the linear evolution of the fluctuations above threshold. The null eigenvalue of this mode allows quantum noise to change the orientation of the bright mode randomly. Though continuously increasing with time, this rotation of the classically excited pattern is quite slow when working above threshold.

(iii) As for the squeezing properties, it has been proved that the bright mode has the same behavior as the single-mode DOPO; that is, perfect squeezing appears only at threshold (within the linearized theory) and degrades fast as the pump is moved apart from this level. On the other hand, accompanying the Goldstone mode it appears another mode whose associated eigenvalue takes the minimum possible value (-2). These modes are responsible for the remarkable properties of the dark mode: Its phase quadrature is perfectly squeezed at any pump level, while its amplitude quadrature carries only with vacuum fluctuations [12] (in apparent violation of the uncertainty principle). A simple explanation of this phenomenon in terms of "angle-angular momentum" uncertainty relation appears once one notices that the dark mode coincides (up to a $\pi/2$ phase) with the OAM of the generated pattern.

(iv) We have proved that the apparent violation of the uncertainty principle is just that—"apparent"—as the conjugate pair of the squeezed quadrature is not another quadrature but the orientation of the bright mode, which in fact is completely undetermined in the long term.

(v) Next we have pointed out that in order to measure the quantum properties of the dark mode, one has to use a TEM_{10} local oscillator that is perfectly matched to the orientation of this mode at any time. However, the mode is rotating randomly, which seems to make perfect matching impossible. For this reason we have studied the situation in which the local oscillator is matched to the dark mode's orientation only at the initial time, remaining fixed during the detection time. We have shown that arbitrarily large levels of noise reduction can be obtained even in this case if the phase of the local oscillator is exactly $\pi/2$. We then considered phase deviations up to 2° (1.5° seems to be the current experimental limit [2,3]), comparing the results with that predicted for the single-mode DOPO; similar levels are obtained for both, with the advantage that in the two-transverse-mode DOPO this level is independent of the distance from threshold, and hence, noncritical.

(vi) In the last part of the article we have shown that the assumptions made in order to analytically solve the problem are not responsible for the quantum properties of the dark mode. In particular, we have shown that when the pump is not adiabatically eliminated, the Goldstone mode and its companion with the lowest possible eigenvalue remain unchanged in the matrix governing the linear evolution of the full problem, and hence all the properties derived from them are still present. Finally, we have used numerical simulations to show that the predictions of the linearized equations are in perfect agreement with those of the full nonlinear equations, and hence the perfect, noncritical squeezing of the dark mode is not a by-product of the linearization.

We believe that the analyses presented in this article (together with the facts that the properties of the dark mode are not too sensitive to imperfections in the rotational symmetry of the DOPO [12] and that the phenomenon is present in other kinds of nonlinear resonators [33,34]) show that that the phenomenon of noncritical squeezing induced by spontaneous rotational symmetry breaking is a robust phenomenon.

An interesting prospect could be to analyze other OPO configurations (like nondegenerate or degenerate type-II operation) when a given family of transverse modes resonates at the relevant frequencies. In connection to these schemes, the classical dynamics of an OPO resonating in the first transverse family at the signal and/or idler frequencies was studied in [35]. The interplay between the usual bipartite entanglement of these configurations with the noncritical quadrature squeezing found in several transverse modes [33,36] could enhance the quantum capabilities of the OPOs.

ACKNOWLEDGMENTS

We thank Ferran V. Garcia–Ferrer for his help in Sec. V A. This work has been supported by the Spanish Ministerio de Educación y Ciencia and the European Union FEDER through Project No. FIS2008-06024-C03-01. C.N.-B. is a grant holder of the FPU program of the Ministerio de Ciencia e Innovación (Spain). A.R. acknowledges financial support from the Universitat de València through its program "Convocatoria de Estancias Temporales para Investigadores Invitados."

APPENDIX A: MODEL AND PHYSICAL PARAMETERS

In the article some parameters have been used to model the DOPO. Here we want to give explicit expressions for them in terms of physical quantities for the case of a DOPO having a Fabry-Perot cavity of effective length L and formed by two identical spherical mirrors with curvature radii R for simplicity. The nonlinear crystal is placed at the waist plane of this cavity and has refractive index n, second-order

susceptibility $\chi^{(2)}$, and axial length l (assumed to be much smaller than the Rayleigh length of the cavity).

For this cavity configuration, the beam radius at the waist plane of the resonator is given by [16]

$$w_j^2 = \frac{\lambda_j L}{2\pi}\sqrt{\frac{2R}{L}-1}, \quad j = \mathrm{p,s}, \tag{A1}$$

where λ_j is the wavelength of the considered mode inside the cavity.

On the other hand, the parameters that appear in the Hamiltonian (9) accounting for the external laser pump and the nonlinear interaction inside the crystal, namely $\mathcal{E}_\mathrm{p}$ and χ, respectively, have the following expression:

$$\begin{aligned} \mathcal{E}_\mathrm{p} &= \sqrt{\frac{n\lambda_\mathrm{p}\gamma_\mathrm{p}}{2\pi\hbar c}P_\mathrm{laser}}, \\ \chi &= \frac{3\pi\chi^{(2)}l}{w_\mathrm{p}}\sqrt{\frac{\hbar}{\varepsilon_0}}\left(\frac{c}{nL\lambda_\mathrm{p}}\right)^{3/2}, \end{aligned} \tag{A2}$$

$\gamma_j = c\mathcal{T}_j/2L$ being the cavity decay rate at the considered frequency ($\mathcal{T}_j$ is the corresponding transmission factor through the input mirror) and P_laser the power of the injected laser. In order to obtain these expressions all the transmitted pump power is assumed to be focalized inside the transverse dimensions of the nonlinear crystal.

Throughout the article, some expressions have been evaluated for concrete system parameters. We have taken as typical parameters the following ones:

$$\begin{array}{llll} \lambda_\mathrm{p} = 400\ \mathrm{nm}, & R = 1\ \mathrm{m}, & \mathcal{T}_\mathrm{p} = 0.1, & \chi^{(2)} = 2\ \frac{\mathrm{pm}}{\mathrm{V}}, \\ L = 0.1\ \mathrm{m}, & l = 1\ \mathrm{mm}, & \mathcal{T}_\mathrm{s} = 0.01, & n = 2.5, \end{array}$$

leading to the following model parameters

$$\begin{array}{ll} w_\mathrm{p} = 167\ \mu\mathrm{m}, & \chi = 64\ \mathrm{s}^{-1}, \\ \gamma_\mathrm{p} = 0.15\ \mathrm{ns}^{-1}, & \gamma_\mathrm{s} = 0.015\ \mathrm{ns}^{-1}. \end{array}$$

Note the smallness of the parameter g (16), which for these parameter choice has a value of 1.3×10^{-6}.

APPENDIX B: CONNECTION BETWEEN FOKKER-PLANCK AND LANGEVIN EQUATIONS

In the article we make extensive use of the equivalence between Langevin and Fokker-Planck equations. In this appendix we want to briefly review this connection.

Consider a set of real variables $\mathbf{x} = (x_1, x_2, \ldots, x_n)$, satisfying stochastic Langevin equations

$$\frac{d\mathbf{x}}{dt} = \mathbf{A}(\mathbf{x}) + \mathcal{B}(\mathbf{x})\boldsymbol{\eta}(t), \tag{B1}$$

where $\mathbf{A}(\mathbf{x})$ and $\mathcal{B}(\mathbf{x})$ are a vector and a matrix which depend on the variables and the components of $\boldsymbol{\eta}(t)$ are real noises satisfying the usual statistical properties (31).

The theory of stochastic processes [37] states that the stochastic average of any function of the variables $f(\mathbf{x})$ can be evaluated as

$$\langle f(\mathbf{x})\rangle_\mathrm{stochastic} = \int d^n\mathbf{x} P(\mathbf{x}) f(\mathbf{x}), \tag{B2}$$

where the probability distribution $P(\mathbf{x})$ satisfies the Fokker-Planck equation

$$\partial_t P(t;\mathbf{x}) = \left[-\sum_i \partial_i A_i^{(\mathrm{FP})} + \frac{1}{2}\sum_{i,j}\partial_{i,j}^2 \mathcal{D}_{ij}\right] P(t;\mathbf{x}), \tag{B3}$$

having drift vector and diffusion matrix

$$A_i^{(\mathrm{FP})} = A_i + \frac{\nu}{2}\sum_{jk}\mathcal{B}_{kj}\partial_k\mathcal{B}_{ij}, \tag{B4}$$

and

$$\mathcal{D} = \mathcal{B}\mathcal{B}^T, \tag{B5}$$

respectively.

The parameter ν is 0 or 1 depending on whether we interpret Eqs. (B1) as Ito or Stratonovich stochastic equations. In the current article any stochastic equation is interpreted à la Stratonovich, which allows us to use the usual rules of calculus. Note that if the extra term involving derivatives of the noise matrix is zero, Ito and Stratonovich interpretations are equivalent, which happens for example in Eqs. (10) but not in Eqs. (22).

APPENDIX C: CONSIDERATIONS ON THE LINEARIZATION PROCEDURE

Following the linearization procedure we explained in Sec. III A leads not to Eq. (25) directly, but to

$$i(\mathcal{G}\mathbf{b} - 2\rho\mathbf{w}_0)\dot{\theta} + \dot{\mathbf{b}} = \mathcal{L}\mathbf{b} + g\mathcal{K}(\theta)\boldsymbol{\zeta}(\tau), \tag{C1}$$

where

$$\begin{aligned} \mathcal{K}(\theta) &= \mathrm{diag}\,(e^{i\theta}, e^{-i\theta}, e^{-i\theta}, e^{i\theta}), \\ \mathcal{G} &= \mathrm{diag}\,(-1,1,1,-1), \end{aligned}$$

and the rest of vectors and symbols were defined in the corresponding section. Note that the differences between this system of equations and the one used in the text (25) are the matrix $\mathcal{K}(\theta)$ and the $i\mathcal{G}\mathbf{b}\dot{\theta}$ term. The latter is of order g^2 (as the b's and $\dot{\theta}$ are of order g), and hence it can be simply removed within the linearized theory.

Understanding why $\mathcal{K}(\theta)$ can be removed from the linearized equations is a little more involved. Projecting these equations onto the eigensystem of $\mathcal{L}$ (28) and defining the vector $\mathbf{c} = \mathrm{col}(\theta, c_1, c_2, c_3)$ leads to the following system of equations (remember that we set $c_0 = 0$):

$$\dot{\mathbf{c}} = -\Lambda\mathbf{c} + g\mathcal{B}\mathcal{R}(\theta)\boldsymbol{\eta}(\tau), \tag{C2}$$

with

$$\begin{aligned} \Lambda &= 2\mathrm{diag}(0,1,\sigma-1,\sigma), \\ \mathcal{B} &= \mathrm{diag}(1/2\rho, i, 1, 1), \\ \mathcal{R}(\theta) &= \mathcal{R}_{1,3}(\theta)\mathcal{R}_{2,4}(-\theta), \end{aligned} \tag{C3}$$

$\mathcal{R}_{i,j}(\theta)$ being the two-dimensional rotation matrix of angle θ acting on the i-j subspace and where the components of vector $\boldsymbol{\eta}(\tau)$ are real, independent noises satisfying the usual statistical properties (31). Now we will prove that this system and the same system but taking $\mathcal{R}(\theta = 0)$, are equivalent within the linearized theory, what implies that (C1) and (25) are equivalent too.

To show this, we just write the Fokker-Planck equation corresponding to this stochastic system (see Appendix B), whose drift vector and diffusion matrix are found to be

$$\mathbf{A} = \Lambda\mathbf{c} + \frac{g^2}{4\rho}\mathrm{col}(0,0,1,0) \tag{C4}$$

and

$$\mathcal{D} = g^2\mathcal{B}\mathcal{B}^T, \tag{C5}$$

respectively. Note that in the previous equation we have used $\mathcal{R}(\theta)$ as an orthogonal matrix.

The proof is completed by writing the stochastic system corresponding to this Fokker-Planck equation up to the linear order in g, which reads

$$\dot{\mathbf{c}} = -\Lambda\mathbf{c} + g\mathcal{B}\boldsymbol{\eta}(\tau), \tag{C6}$$

corresponding to (C2) with $\mathcal{R}(\theta = 0)$ as we wanted to prove.

Hence, removing $\mathcal{K}(\theta)$ and neglecting the $i\mathcal{G}\mathbf{b}\dot{\theta}$ term from (C1) does not change its equivalent Fokker-Planck equation within the linearized description, and thus Eq. (25) must lead to the same predictions as (C1).

APPENDIX D: LINEAR LANGEVIN EQUATIONS: SOLUTION, CORRELATION AND SPECTRUM

In this appendix we solve the linear evolution equations (29) of the projections c_m, finding their two-time-correlation function and the associated spectrum. These equations are of the general type

$$\dot{c} = -\lambda c + \Gamma\eta(\tau), \tag{D1}$$

where $\eta(\tau)$ is a real noise satisfying the usual white-noise statistics (31), λ is a real, positive parameter, and Γ is a parameter that might be complex.

By making the variable change $z(\tau) = c(\tau)\exp(\lambda\tau)$, and considering times larger that λ^{-1} (stationary limit), it is straightforward to find the following solution:

$$c(\tau) = \Gamma\int_0^\tau d\tau_1\eta(\tau_1)e^{\lambda(\tau_1-\tau)}. \tag{D2}$$

From the statistical properties of noise (31), we see that this solution has zero mean, $\langle c(\tau)\rangle = 0$, and correlation

$$\langle c(\tau)c(\tau')\rangle = \Gamma^2 e^{-\lambda(\tau+\tau')} \times \int_0^\tau d\tau_1\int_0^{\tau'} d\tau_2\delta(\tau_1-\tau_2)e^{\lambda(\tau_1+\tau_2)}. \tag{D3}$$

Considering separately the cases $\tau' > \tau$ and $\tau' < \tau$, this integral is easily carried out, yielding (again the limit $\tau \gg \lambda^{-1}$ is considered)

$$\langle c(\tau)c(\tau')\rangle = \frac{\Gamma^2}{2\lambda}e^{-\lambda|\tau'-\tau|}, \tag{D4}$$

where we see that this function depends only on the time difference $|\tau' - \tau|$, which justifies the name "stationary limit" for the $\tau \gg \lambda^{-1}$ approximation.

Finally, the spectrum of this correlation is found to be

$$\tilde{C}(\omega) = \int_{-\infty}^{+\infty} d\bar{\tau}e^{-i\omega\bar{\tau}}\langle c(\tau)c(\tau+\bar{\tau})\rangle = \frac{\Gamma^2}{\lambda^2+\omega^2}. \tag{D5}$$

Hence, particularized to the equations for the projections c_m (IV A), the correlations read

$$\begin{aligned}\langle c_1(\tau)c_1(\tau')\rangle &= -\frac{g^2}{4}e^{-2|\tau'-\tau|},\\ \langle c_2(\tau)c_2(\tau')\rangle &= \frac{g^2}{4(\sigma-1)}e^{-2(\sigma-1)|\tau'-\tau|},\\ \langle c_3(\tau)c_3(\tau')\rangle &= \frac{g^2}{4\sigma}e^{-2\sigma|\tau'-\tau|},\end{aligned} \tag{D6}$$

while the spectra read

$$\begin{aligned}\tilde{C}_1(\omega) &= -\frac{g^2}{4+\omega^2},\\ \tilde{C}_2(\omega) &= \frac{g^2}{4(\sigma-1)^2+\omega^2},\\ \tilde{C}_3(\omega) &= \frac{g^2}{4\sigma^2+\omega^2},\end{aligned} \tag{D7}$$

and the stationary limit is reached when $\tau \gg 0.5$, $\tau \gg 0.5(\sigma-1)^2$ and $\tau \gg 0.5\sigma^{-1}$, respectively.

APPENDIX E: CALCULATING CORRELATIONS FOR THE UNDAMPED ORIENTATION θ

In this appendix we show how $S(\tau_1,\tau_2)$ and $C(\tau_1,\tau_2)$ defined in (53) can be evaluated from the evolution equation of θ (29a). As clearly explained in [38], this equation defines a Wiener or random walk process equivalently described by the following Fokker-Planck equation:

$$\partial_\tau P(\theta,\tau) = \tfrac{1}{2}D\partial_\theta^2 P(\theta,\tau). \tag{E1}$$

In the same reference, it is also proved that the two-time joint probability associated to this simple diffusion equation is

$$P(\theta_2,\tau_2;\theta_1,\tau_1) = \frac{1}{2\pi D\sqrt{\tau_1(\tau_2-\tau_1)}}e^{-\frac{1}{2D}\left[\frac{(\theta_2-\theta_1)^2}{\tau_2-\tau_1}+\frac{\theta_1^2}{\tau_1}\right]}, \tag{E2}$$

which gives us the probability of passing from orientation θ_1 at time τ_1 to θ_2 at time τ_2 (it is assumed that $\theta = 0$ at the initial time $\tau = 0$). Of course, in this expression $\tau_2 > \tau_1$. From this joint probability the correlations are calculated as the integrals

$$\begin{aligned}S(\tau_1,\tau_2) &= \int\int_{-\infty}^{+\infty} d\theta_1 d\theta_2 P(\theta_2,\tau_2;\theta_1,\tau_1)\sin\theta_1\sin\theta_2,\\ C(\tau_1,\tau_2) &= \int\int_{-\infty}^{+\infty} d\theta_1 d\theta_2 P(\theta_2,\tau_2;\theta_1,\tau_1)\cos\theta_1\cos\theta_2.\end{aligned} \tag{E3}$$

These integrals are easily evaluated, yielding

$$S(\tau_1,\tau_2) = e^{-\frac{1}{2}D(\tau_1+\tau_2)}\sinh[D\min(\tau_1,\tau_2)] \tag{E4}$$

and

$$C(\tau_1,\tau_2) = e^{-\frac{1}{2}D(\tau_1+\tau_2)}\cosh[D\min(\tau_1,\tau_2)]. \tag{E5}$$

APPENDIX F: DETAILS OF THE NUMERICAL SIMULATION

In this final appendix we want to briefly resume the details concerning the numerical simulation of the Langevin equations (15).

The first important property of these equations is that, irrespective of the initial conditions, the amplitudes corresponding to opposite OAM modes become complex conjugate after a short transitory time; that is, $(\beta_{-1},\beta_{-1}^{+}) \to (\beta_{+1}^{*},[\beta_{+1}^{+}]^{*})$. Hence, if the initial conditions are chosen so that the OAM pairs are complex conjugate, we can be sure that they will remain complex conjugate during the evolution. In particular, we have chosen the above-threshold stationary solution (20) with $\theta = 0$ as the initial condition. Under these conditions, the six Langevin equations (15) reduce to the following four (which we write in matrix form):

$$\dot{\boldsymbol{\beta}} = \mathbf{A}(\boldsymbol{\beta}) + \mathcal{B}(\boldsymbol{\beta}) \cdot \boldsymbol{\zeta}(\tau), \tag{F1}$$

with

$$\boldsymbol{\beta} = \begin{pmatrix} \beta_0 \\ \beta_0^{+} \\ \beta_{+1} \\ \beta_{+1}^{+} \end{pmatrix}, \qquad \boldsymbol{\zeta}(\tau) = \begin{pmatrix} 0 \\ 0 \\ \zeta(\tau) \\ \zeta^{+}(\tau) \end{pmatrix}, \tag{F2}$$

$$\mathbf{A}(\boldsymbol{\beta}) = \begin{pmatrix} \sigma - \beta_0 - |\beta_{+1}|^2 \\ \sigma - \beta_0^{+} - |\beta_{+1}^{+}|^2 \\ -\beta_{+1} + \beta_0[\beta_{+1}^{+}]^{*} \\ -\beta_{+1}^{+} + \beta_0^{+}\beta_{+1}^{*} \end{pmatrix},$$

$$\mathcal{B}(\boldsymbol{\beta}) = g\,\mathrm{diag}\,(0,0,\sqrt{\beta_0},\sqrt{\beta_0^{+}}).$$

In order to solve numerically these equations, we use the semi-implicit algorithm developed in Ref. [32]. This algorithm is a finite-differences-based method in which the total integration time τ_{end} (the integration is supposed to begin always at $\tau = 0$) is divided into N segments, creating hence a lattice of times $\{\tau_n\}_{n=0,1,\ldots,N}$ separated by time steps $\Delta\tau = \tau_{\mathrm{end}}/N$. Then, a recursive algorithm starts in which the amplitudes at time τ_n, say $\boldsymbol{\beta}_n$, are found from the amplitudes $\boldsymbol{\beta}^{n-1}$ at an earlier time τ_{n-1} from

$$\boldsymbol{\beta}^{n} = \boldsymbol{\beta}^{n-1} + \Delta\tau\mathbf{A}(\tilde{\boldsymbol{\beta}}^{n}) + \mathcal{B}(\tilde{\boldsymbol{\beta}}^{n}) \cdot \mathbf{W}^{n}, \tag{F3}$$

where $\tilde{\boldsymbol{\beta}}^{n}$ is an approximation to the amplitudes at the midpoint between τ_{n-1} and τ_n (hence the name "semi-implicit" for the algorithm) and the components of $\mathbf{W}^{n}$ are independent discrete noises W_j^{n} with null mean and satisfying the correlations

$$\langle W_j^{m},[W_k^{n}]^{*}\rangle = \Delta\tau\delta_{mn}\delta_{jk}. \tag{F4}$$

The midpoint approximation is found from the following iterative algorithm:

$$\tilde{\boldsymbol{\beta}}^{n,p} = \boldsymbol{\beta}^{n-1} + \tfrac{1}{2}[\Delta\tau\mathbf{A}(\tilde{\boldsymbol{\beta}}^{n,p-1}) + \mathcal{B}(\tilde{\boldsymbol{\beta}}^{n,p-1}) \cdot \mathbf{W}^{n}], \tag{F5}$$

where $\tilde{\boldsymbol{\beta}}^{n,0} = \boldsymbol{\beta}^{n-1}$, p being the iteration index (two iterations are carried in our simulations), while the discrete noises can be simulated at any step as [39]

$$W_j^{n} = \sqrt{\Delta\tau}[r(z_j,z_j') + ir(y_j,y_j')], \tag{F6}$$

with

$$r(z,z') = \sqrt{-\ln z}\cos(2\pi z'), \tag{F7}$$

z_j,z_j',y_j, and y_j' being independent random numbers uniformly distributed along the interval $[0,1]$.

This algorithm allows us to simulate one stochastic trajectory. Then, by repeating it Σ times, the stochastic average of any function can be approximated by the arithmetic mean of the values of that function evaluated at the different stochastic trajectories.

[1] P. Meystre and D. F. Walls (editors), *Nonclassical Effects in Quantum Optics* (American Institute of Physics, New York, 1991).

[2] H. Vahlbruch, M. Mehmet, S. Chelkowski, B. Hage, A. Franzen, N. Lastzka, S. Gossler, K. Danzmann, and R. Schnabel, Phys. Rev. Lett. **100**, 033602 (2008); see also M. Mehmet, H. Vahlbruch, N. Lastzka, K. Danzmann, and R. Schnabel, Phys. Rev. A **81**, 013814 (2010).

[3] Y. Takeno, M. Yukawa, H. Yonezawa, and A. Furusawa, Opt. Express **15**, 4321 (2007)

[4] M. J. Collett and C. W. Gardiner, Phys. Rev. A **30**, 1386 (1984).

[5] S. Chaturvedi, K. Dechoum, and P. D. Drummond, Phys. Rev. A **65**, 033805 (2002).

[6] S. L. Braunstein and P. van Loock, Rev. Mod. Phys. **77**, 513 (2005).

[7] P. van Loock and S. L. Braunstein, Phys. Rev. Lett. **84**, 3482 (2000); T. Aoki, N. Takei, H. Yonezawa, K. Wakui, T. Hiraoka, A. Furusawa, and P. vanLoock, *ibid.* **91**, 080404 (2003).

[8] N. Treps, U. Andersen, B. Buchler, P. K. Lam, A. Mâitre, H. A. Bachor, and C. Fabre, Phys. Rev. Lett. **88**, 203601 (2002); N. Treps, N. Grosse, W. P. Bowen, C. Fabre, H.-A. Bachor, and P. K. Lam, Science **301**, 940 (2003).

[9] H. Vahlbruch, S. Chelkowski, B. Hage, A. Franzen, K. Danzmann, and R. Schnabel, Phys. Rev. Lett. **95**, 211102 (2005); K. Goda, O. Miyakawa, E. E. Mikhailov, S. Saraf, R. Adhikari, K. McKenzie, R. Ward, S. Vass, A. J. Weinstein, and N. Mavalvala, Nat. Phys. **4**, 472 (2008).

[10] I. Pérez-Arjona, E. Roldán, and G. J. de Valcárcel, Europhys. Lett. **74**, 247 (2006); Phys. Rev. A **75**, 063802 (2007).

[11] K. Staliunas and V. J. Sánchez-Morcillo, Opt. Commun. **139**, 306 (1997); S. Longhi, Phys. Scr. **56**, 611 (1997).

[12] C. Navarrete-Benlloch, E. Roldán, and G. J. de Valcárcel, Phys. Rev. Lett. **100**, 203601 (2008).

[13] We would like to note that experiments related to this DOPO's configuration have been recently performed below threshold [14].

[14] M. Lassen, G. Leuchs, and U. L. Andersen, Phys. Rev. Lett. **102**, 163602 (2009); J. Janousek, K. Wagner, J.-F. Morizur, N. Treps, P. K. Lam, C. C. Harb, and H.-A. Bachor, Nat. Photonics **3**, 399 (2009).

[15] C. Navarrete-Benlloch, E. Roldán, and G. J. de Valcárcel, e-print arXiv:0802.4356.

[16] N. Hodgson and H. Weber, *Laser Resonators and Beam Propagation* (Springer, New York, 2005).

[17] C. W. Gardiner and P. Zoller, *Quantum Noise* (Springer, New York, 2000).

[18] K. J. McNeil and C. W. Gardiner, Phys. Rev. A **28**, 1560 (1983).

[19] S. Reynaud, C. Fabre, and E. Giacobino, J. Opt. Soc. Am. B **4**, 1520 (1987); A. Heidmann, R. J. Horowicz, S. Reynaud, E. Giacobino, C. Fabre, and G. Camy, Phys. Rev. Lett. **59**, 2555 (1987); A. S. Lane, M. D. Reid, and D. F. Walls, Phys. Rev. A **38**, 788 (1988).

[20] M. D. Reid and P. D. Drummond, Phys. Rev. Lett. **60**, 2731 (1988); Phys. Rev. A **40**, 4493 (1989).

[21] H. J. Carmichael, *Statistical Methods in Quantum Optics* (Springer, Berlin, 1999), Vol. 1.

[22] P. D. Drummond and C. W. Gardiner, J. Phys. A **13**, 2353 (1980).

[23] S. Feng and O. Pfister, J. Opt. B: Quantum Semiclass. Opt. **5**, 262 (2003); J. Jing, S. Feng, R. Bloomer, and O. Pfister, Phys. Rev. A **74**, 041804(R) (2006).

[24] L. Longchambon, J. Laurat, T. Coudreau, and C. Fabre, Eur. Phys. J. D **30**, 287 (2004); J. Laurat, L. Longchambon, C. Fabre, and T. Coudreau, Opt. Lett. **30**, 1177 (2005).

[25] G. J. de Valcárcel (unpublished).

[26] K. Dechoum, P. D. Drummond, S. Chaturvedi, and M. D. Reid, Phys. Rev. A **70**, 053807 (2004).

[27] Note that the quantitative difference between this diffusion coefficient D and that of [12], named D_θ in that reference, comes from the fact that D is D_θ normalized to γ_s.

[28] J. Gea-Banacloche, N. Lu, L. M. Pedrotti, S. Prasad, M. O. Scully, and K. Wódkiewicz, Phys. Rev. A **41**, 369 (1990).

[29] A. Luis and L. L. Sánchez-Soto, Phys. Rev. A **48**, 4702 (1993); S. Yu, Phys. Rev. Lett. **79**, 780 (1997).

[30] In the single-mode DOPO the best levels of squeezing are found below threshold (within the linearized theory), where its noise spectrum can be written as $V^{\rm out}(\omega) = 1 + S_+(\omega)\cos^2\varphi - S_-(\omega)\sin^2\varphi$, with $S_\pm(\omega) = 4\sigma/[(\sigma \pm 1)^2 + \omega^2]$.

[31] This means that there exists a set of eigenvectors $\mathbf{v}_m$ satisfying $\mathcal{L}\mathbf{v}_m = \lambda_m \mathbf{v}_m$, and another set $\mathbf{w}_m$ satisfying $\mathcal{L}^\dagger \mathbf{w}_m = \lambda_m^* \mathbf{w}_m$, so that $\mathbf{w}_m^* \cdot \mathbf{v}_m = \delta_{mn}$.

[32] P. D. Drummond and I. K. Mortimer, J. Comput. Phys. **93**, 144 (1991).

[33] C. Navarrete-Benlloch, G. J. de Valcárcel, and E. Roldán, Phys. Rev. A **79**, 043820 (2009).

[34] F. V. Garcia-Ferrer, C. Navarrete-Benlloch, G. J. de Valcárcel, and E. Roldán, IEEE J. Quantum Electron. **45**, 1404 (2009).

[35] M. Martinelli, J. A. O. Huguenin, P. Nussenzveig, and A. Z. Khoury, Phys. Rev. A **70**, 013812 (2004); B. Coutinho dos Santos, C. E. R. Souza, K. Dechoum, and A. Z. Khoury, *ibid.* **76**, 053821 (2007).

[36] An experiment proving the main result of [33], namely, the noncritical squeezing in the nonamplified modes, has been recently reported; see B. Chalopin, F. Scazza, C. Fabre, and N. Treps, e-print arXiv:0912.4212.

[37] C. Gardiner, *Stochastic Methods* (Springer, Berlin, 2009), 4th ed.

[38] L. Mandel and E. Wolf, *Optical Coherence and Quantum Optics* (Cambridge University Press, New York, 1995).

[39] R. F. Fox, I. R. Gatland, R. Roy, and G. Vemuri, Phys. Rev. A **38**, 5938 (1988).